© 2022. Published by The Company of Biologists Ltd | Development (2022) 149, dev199985. doi:10.1242/dev.199985

RESEARCH REPORT

Molecular divergence of mammalian astrocyte progenitor cells at early gliogenesis

Jiancheng Liu[1,*], Xiwei Wu[2,*] and Qiang Lu[1,‡]

ABSTRACT

During mammalian brain development, how different astrocytes are specified from progenitor cells is not well understood. In particular, whether astrocyte progenitor cells (APCs) start as a relatively homogenous population or whether there is early heterogeneity remains unclear. Here, we have dissected subpopulations of embryonic mouse forebrain progenitors using single-cell transcriptome analyses. Our sequencing data revealed two molecularly distinct APC subgroups at the start of gliogenesis from both dorsal and ventral forebrains. The two APC subgroups were marked, respectively, by specific expression of *Sparc* and *Sparcl1*, which are known to function in mature astrocytes with opposing activities for regulating synapse formation. Expression analyses showed that SPARC and SPARCL1 mark APC subgroups that display distinct temporal and spatial patterns, correlating with major waves of astrogliogenesis during development. Our results uncover an early molecular divergence of APCs in the mammalian brain and provide a useful transcriptome resource for the study of glial cell specification.

KEY WORDS: Neural progenitor cell heterogeneity, Astrocyte progenitor cell divergence, Gliogenesis, Brain development, SPARC, SPARCL1

INTRODUCTION

Astrocytes are one of the most abundant cell types in the mammalian brain and play crucial functions in supporting and protecting brain organization as well as regulating neuronal circuits formation (Clarke and Barres, 2013; Sloan and Barres, 2014; Ben Haim and Rowitch, 2017). These multiple functions are conceivably executed by different types of astrocytes that are initially specified from progenitor cells during embryonic and early postnatal brain development; however, much of the detail of such developmental programs remains elusive. During development of the mammalian brains, neurons and glial cells are generated by neural progenitor cells (NPCs) in an orderly sequence with neurogenesis preceding gliogenesis. The majority of the main subtypes of cortical projection neurons are sequentially generated during neurogenesis by NPCs, which become progressively restricted in their differentiation potentials from producing early-born neurons to late-born neurons (Gotz and Huttner, 2005; Leone et al., 2008; Kriegstein and Alvarez-Buylla, 2009; Greig et al., 2013). As neurogenesis tapers down, generation of astrocytes becomes increasingly more prominent. However, when compared with our understanding of neuronal specification during neurogenesis, the developmental regulation of astrogliogenesis and subtype specification are only beginning to be addressed (Bayraktar et al., 2014; Tabata, 2015; Akdemir et al., 2020).

Recently, diverse subtypes of mature astrocytes associated with distinct neocortical layers or brain regions were identified in the adult mouse brains (John Lin et al., 2017; Lanjakornsiripan et al., 2018; Batiuk et al., 2020; Bayraktar et al., 2020). It is conceivable that specification of these subtypes of astrocytes in the brain may use a similar progressive restriction mechanism of progenitors, involve early lineage-restricted progenitors or rely on local environmental cues, or a combination of these factors (Rowitch and Kriegstein, 2010; Molofsky and Deneen, 2015; Khakh and Deneen, 2019). Previous studies of astrocyte development in the mouse spinal cord identified two morphologically distinct types of early astrocyte precursors that were subjected to temporal and spatial control (Tien et al., 2012), suggesting that astrocytes could be produced from fate-specified progenitors present during early gliogenesis. In the mouse brains, glial progenitor cell diversity was also observed in juvenile and adult mice (Marques et al., 2016; Weng et al., 2019); however, whether astrocyte progenitor cells (APCs) start as a relatively homogeneous pool or whether different subgroups of progenitors can co-initiate astrocyte production is unclear. If heterogeneity of APCs emerges early in the brain, whether such subtypes of progenitors are present as an intermixed population or whether they can display temporally and/or spatially defined patterns also remain to be determined. Answering these questions requires a detailed analysis of neural progenitor cell heterogeneity at the start of gliogenesis.

Single-cell RNA sequencing (scRNA-seq) technology provides a powerful tool for dissecting the heterogeneity of cell populations. Multiple studies have performed single cell analyses with either mouse or human cortical cells, and the results have documented heterogeneity within the NPC or neuron populations (Johnson et al., 2015; Pollen et al., 2015; Shin et al., 2015; Zeisel et al., 2015, 2018; Okamoto et al., 2016; Yuzwa et al., 2017; Mi et al., 2018; Zhong et al., 2018; Telley et al., 2019; Loo et al., 2019; Polioudakis et al., 2019; Li et al., 2020). Because many of these studies sequenced brain tissues of a mixed cell population, the low percentage of NPCs in total brain cells presented a challenge for a detailed characterization of heterogeneity and molecular markers specifically associated with the NPC population if not enough total brain cells were analyzed. To dissect heterogeneity of NPCs more comprehensively during brain development, we employed an established approach for purification of NPCs from the *Nes-GFP/Dcx-mRFP* double transgenic reporter mice. Bulk sequencing using the system has verified that the transcriptomes of NPCs are faithfully preserved after purification (Wang et al., 2011; Hahn et al., 2013; Liu et al., 2017, 2018). In addition, we profiled

[1]Department of Developmental and Stem Cell Biology, Beckman Research Institute of City of Hope, Duarte, CA 91010, USA. [2]Department of Molecular and Cellular Biology, Beckman Research Institute of City of Hope, Duarte, CA 91010, USA.
*These authors contributed equally to this work

‡Author for correspondence (qlu@coh.org)

Q.L., 0000-0001-5753-9988

Handling Editor: James Briscoe
Received 6 July 2021; Accepted 26 January 2022

Development (2022) 149, dev199985. doi:10.1242/dev.199985

single-cell transcriptomes of purified NPCs from two developmental stages at the neurogenesis-to-gliogenesis transition to better reveal the emerging glial progenitor cell population. Here, we report that the scRNA-seq data revealed multiple clusters of NPCs, among which two molecularly distinct subgroups of APCs were identified. The presence of these APC subgroups and their respective developmental expression patterns were further characterized by analyzing specific markers during early gliogenesis.

RESULTS AND DISCUSSION

Identification of two distinct astrocyte progenitor subgroups from cortical NPCs by scRNA-seq

Purification of NPCs from the *Nes-GFP/Dcx-mRFP* double transgenic reporter mice was combined with the 10X Chromium platform to obtain single-cell transcriptomes (Fig. 1A). NPCs (GFP^+RFP^- cells, Fig. S1) were purified from the cortices at embryonic day 15.5 (E15.5; peak neurogenesis stage) and E18.5 (end neurogenesis/early gliogenesis stage). After quality control and filtering, 878 cells at E15.5 and 1150 cells at E18.5 were used for subsequent analyses. The 1325 most variable genes were selected, and the top 11 principal components (PCs) were used in the plot analysis. The results could clearly delineate ten cell clusters (cluster 0 to cluster 9 inclusive), within which the E18.5 cortex contained more cell clusters than the E15.5 cortex (Fig. 1B-E).

Heatmap results showed that the ten clusters were marked by differential expression patterns of representative genes (Fig. 1D). Cluster 1 was the group of intermediate progenitor cells (IPCs), marked by the expression of *Eomes/Tbr2*. Clusters 2 and 4 were cycling progenitors enriched with cell-cycle related genes such as *Ccnb1*, *Ccnb2* and *Cdc20*. Interestingly, the data revealed three clusters of glial cell lineages prominently enriched in the E18.5 cortices. These included two astrocyte progenitor cell (APC) subgroups (clusters 5 and 7) expressing *Aldh1l1, Slc1a3* and *Fabp7* in both groups (Fig. 1D,F), and an oligodendrocyte progenitor cell (OPC) subgroup (cluster 3) expressing most known OPC markers, such as *Olig1*, *Olig2*, *Pdgfra* and *Sox8* (Fig. 1D). Between the two APC subgroups (Fig. 1F,G), *Sparc* and *Sparcl1* transcripts were specifically enriched in cluster 5 and cluster 7 cells, respectively (Fig. 1D). Cluster 5 showed relatively higher expressions of metallothionein (MT) family members *Mt1*, *Mt2* and *Mt3*, while cluster 7 had higher expression of *Olig1*, *Olig2* and *Egfr* (Fig. 1D,F, Fig. S2). Cluster 6 is a population expressing interneuron lineage-specific markers, such as *Lhx6* and *Arx*, etc. (Fig. 1D,E), representing the differentiating interneuron progenitors that migrated tangentially into the cortex from the ventral forebrain (Anderson et al., 1997; Wu et al., 2011). The sequencing data also included a small group of projection neurons (cluster 8) and endothelial lineage cells (cluster 9) (Fig. 1E). The former likely resulted from the stringency of gating during FACS purification of NPCs; the latter might be co-isolated due to expression of *Nes-GFP* in proliferating endothelial cells (Suzuki et al., 2010). Unlike other clusters with distinct markers, cells of cluster 0 express relatively high *Eomes*, *Tubb3* and *Fabp7*, but not other differentiated markers or cell cycle-related genes, representing a pro-neuronal and quiescent progenitor cell group, which are likely related to the embryonic cells of origin of the adult subventricular zone (SVZ) neural stem cells (Fuentealba et al., 2015).

Two astrocyte progenitor subgroups identified from the ventral forebrain

Previous studies (Hochstim et al., 2008; Tsai et al., 2012) have shown that astrocytes are generated and allocated to a region associated with their original birth place. To examine whether the two APC subgroups identified in the cortex are present in other brain regions, we purified and sequenced 3602 NPCs (1119 at E15.5 and 2483 at E18.5) from the ganglionic eminence regions of the ventral forebrain (Fig. S3A,B). Interestingly, two similar APC subgroups (cluster 5 and 7) could also be detected in the ganglionic eminence (Fig. S3C,D). The two subgroups of APCs were similarly marked by *Sparc* and *Sparcl1*, respectively (Fig. S3C,E). In addition, they were also differentially enriched with some other specific genes: *Clu*, *Mt3*, *Aldoc* and *Apoe* were associated with *Sparc*-specific lineage, while *Slc1a3*, *Id3*, *Ptn* and *Hes5* were enriched in *Sparcl1*-specific lineage (Fig. S3E). Interestingly, further cell clustering analysis between the cortex and ganglionic eminence showed that the astrocyte lineage progenitors expressing *Sparc* or *Sparcl1* were clustered together, irrespective of their forebrain regions (Fig. S3F). These results collectively indicated that distinct subgroups of APCs were present in both the dorsal and ventral forebrains, and that this molecular divergence started from the early stage of gliogenesis.

Differentially expressed genes between the two APC subgroups in the cortex

To identify potential molecules that can specifically mark the two APC subgroups, we analyzed differential gene expression patterns between the APC subgroups from the cortex. As expected, *Sparc* and *Sparcl1* were shown to specifically identify with APC1 and APC2 subgroups, respectively (Fig. S4A,B). The APC1 subgroup also saw enrichment of *Clu* (cluster 5, Fig. 1F) and *Ptx3* (Fig. S4A, C). The APC2 subgroup was associated with higher expression of the metabotropic glutamate receptor (mGluR) members *Grm3* and *Grm5* (Fig. S4B). In addition, higher expression of Id (inhibitor of DNA binding) family members *Id1*, *Id2* and *Id3* (Fig. S4B,C) was also detected in APC2 subgroup.

SPARC or SPARCL1 expression patterns during brain development

To further examine the two subgroups of APCs, we performed immunostaining of SPARC and SPARCL1 proteins in the mouse brain. Antibody staining showed that SPARC protein was expressed lining the lateral ventricle as early as E16.5 (Fig. 2A). SPARC antibody detected radial processes apparently associated with the ventricular APCs. This was initially seen in the ganglionic eminence from E16.5 (Fig. S5A), but later also became evident in the cortex (Fig. 2B). At later neurogenesis stages, some $SPARC^+$ cells were detected outside the ventricular zone (VZ) in the cortex (Fig. S5B). These cells were presumably the differentiating astrocytes generated by the $SPARC^+$ APCs of the VZ. Between *Sparc*-expressing (cluster 5) and *Sparcl1*-expressing (cluster 7) subgroups, the *Sparc*-expressing subgroup showed higher levels of expression of *Pax6*, suggesting that $SPARC^+$ APCs might be derived from radial glial cells. On the other hand, both cluster 5 and 7 subgroups showed similar expression levels of other progenitor cell markers: *Sox2* and *Nes* (Fig. 2C, Fig. S5C). *Sox2* was also prominent in interneuron-lineage cells (Fig. S5C, cluster 6 versus cluster 8), consistent with previously reported results based on bulk RNA-sequencing (Liu et al., 2016). The *Sparc*-marked APC1 subgroup also showed enriched expression of *Clu* (Fig. 1F; Fig. S4A), and we found that CLU protein was detected lining the ventricle at E18.5 (Fig. S5D), similar to the SPARC staining pattern.

Unlike SPARC, SPARCL1 was mainly detected in cells around two discrete locations: the pallium-subpallium boundary (PSB) in the dorsal forebrain; and the septum-subpallium junction in the

Development (2022) 149, dev199985. doi:10.1242/dev.199985

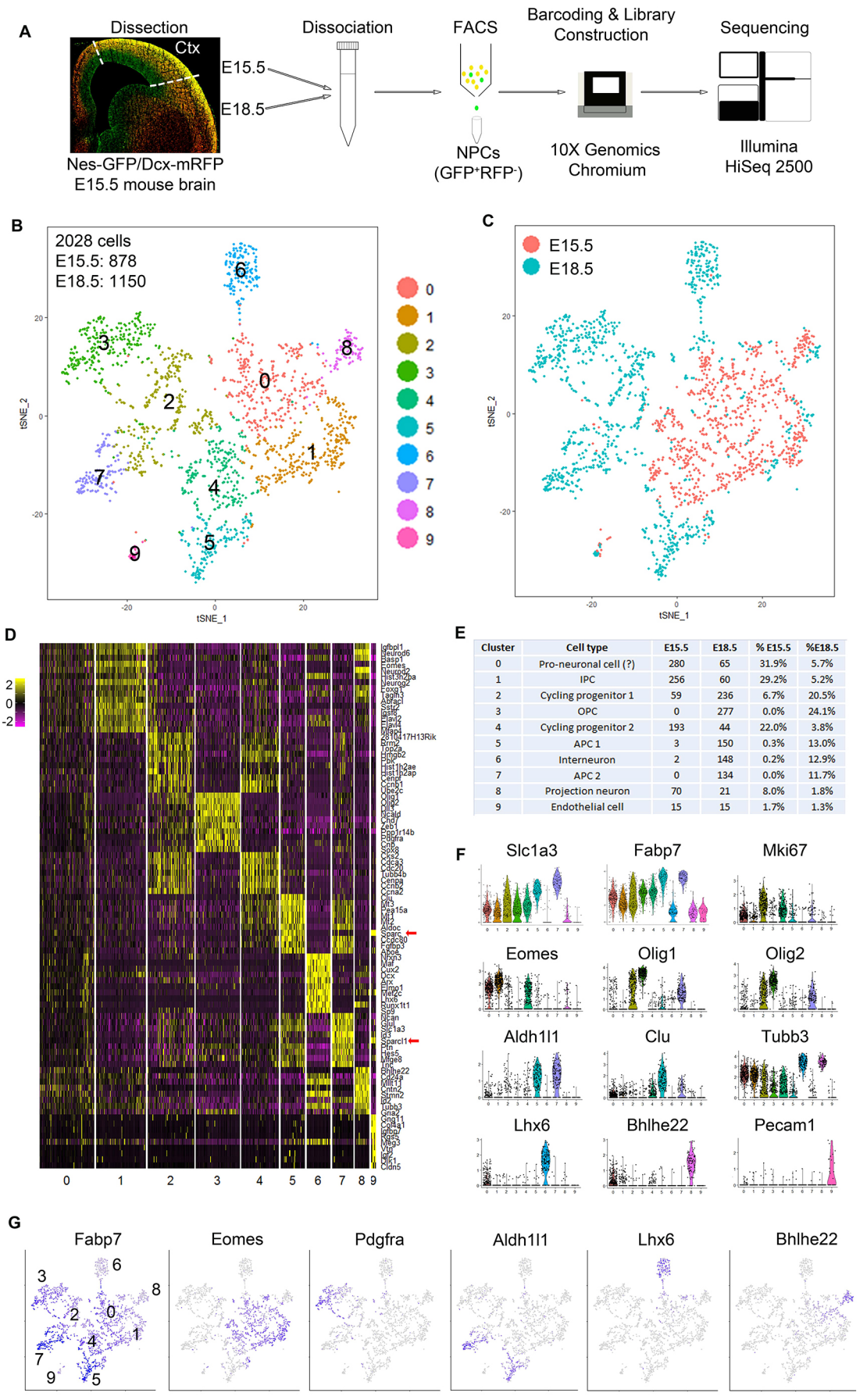

Cluster	Cell type	E15.5	E18.5	% E15.5	%E18.5
0	Pro-neuronal cell (?)	280	65	31.9%	5.7%
1	IPC	256	60	29.2%	5.2%
2	Cycling progenitor 1	59	236	6.7%	20.5%
3	OPC	0	277	0.0%	24.1%
4	Cycling progenitor 2	193	44	22.0%	3.8%
5	APC 1	3	150	0.3%	13.0%
6	Interneuron	2	148	0.2%	12.9%
7	APC 2	0	134	0.0%	11.7%
8	Projection neuron	70	21	8.0%	1.8%
9	Endothelial cell	15	15	1.7%	1.3%

Fig. 1. See next page for legend.

Development (2022) 149, dev199985. doi:10.1242/dev.199985

Fig. 1. Two astrocyte progenitor subgroups identified from the cortex by scRNA-seq. (A) Illustration of purification and processing of cortical NPCs for 10X Genomics single-cell RNA-seq. Image shows *Nes-GFP*/*Dcx-mRFP* brain section at E15.5. Ctx, cortex. (B) t-SNE (t-distributed stochastic neighbor embedding) plot of 2028 single cells at E15.5 and E18.5. The 1325 most variable genes were selected, and top 11 principal components (PCs) were used. (C) t-SNE plot of single cells at E15.5 and E18.5. (D) Heatmap of the single-cell clusters. Representative genes of each cluster are shown. *Sparc* and *Sparcl1* are marked (red arrows). (E) Summary of cell types, cell numbers and ratios at E15.5 and E18.5. IPC, intermediate progenitor cell; OPC, oligodendrocyte progenitor cell; APC, astrocyte progenitor cell. Question mark indicates uncertain. (F) Violin plots of cell type-specific genes. (G) t-SNE plots of marker genes for the subgroups.

ventral forebrain (Fig. 2D; E16.5). In the dorsal brains, SPARCL1$^+$ APCs emerged as early as E16.5, with the staining signals originating at the PSB site and gradually spreading medially to the cortical ventricular zone (VZ) at later stages (e.g. P1) (Fig. 2D; P1), concomitant with SPARCL1$^+$ astrocytes (over 96% SPARCL1$^+$ cells were SOX9$^+$) accumulating in the cortex (Fig. S6). In the ventral brains, SPARCL1$^+$ astrocytes were mostly absent in the ganglionic eminence and septum (areas surrounding the lateral ventricle) but were distributed outside (lateral to) the ganglionic eminence, apparently along the ventral extension of the pallium and in the area ventral to the septum-subpallium junction (Fig. 2D; E18.5 and P1).

Temporal patterns of *Sparc*- and *Sparcl1*-expressing APC subgroups

Because available antibodies were from the same species, we further examined temporal and spatial expression patterns of *Sparc* and *Sparcl1* by co-staining using RNAscope. Like the protein patterns, *Sparc* was expressed along the ventricular zone, whereas *Sparcl1* was detected in dorsolateral SVZ region at E16.5 (Fig. 3A). At E18.5, *Sparcl1* expression gradually extended into the dorsal cortex (Fig. 3B). Cells expressing *Sparcl1* or *Sparc* were distributed in an intermixed pattern (only blood vessel cells co-expressed *Sparcl1* and *Sparc*) (Fig. 3C). To assess their temporal origins in the cortex, we performed developmental trajectory analyses and cluster-specific genes pseudotime analyses. The results showed that NPCs differentiated mainly into neuronal lineage at E15.5 but more prominently into glial lineage at E18.5 (Fig. 3D,E). Consistent with the expression patterns of protein and RNA, SPARC-marked APC1 showed up earlier than SPARCL1-marked APC2 in developmental trajectory (Fig. 3F), and APC1-related genes were expressed earlier in pseudotime (Fig. S7).

Distinct APC subgroups marked by SPARC and SPARCL1 at early gliogenesis

To validate that SPARC- or SPARCL1-marked cells are astrocyte progenitors, we analyzed the expression of these two proteins using the *Aldh1L1-EGFP* reporter mouse line. At early gliogenesis stage E16.5, EGFP signals in the *Aldh1L1-EGFP* reporter brain were seen lining the entire ventricular zone (VZ), as well as at the SVZ along the PSB. SPARC antibody staining showed that expression of SPARC protein and reporter EGFP were positively correlated at the VZ (Fig. 4A-D). In the ganglionic eminence region, SPARC staining revealed processes extending away from the VZ; however, no long processes could be detected in the cortex at this stage, indicating that SPARC$^+$ astrocyte progenitors emerged earlier in the ganglionic eminence than in the cortex. Although SPARC signal was absent at the region along the PSB, SPARCL1 signal could be prominently detected in this location marked by EGFP reporter (Fig. 4E,F). These results further confirmed that SPARC and SPARCL1 mark two distinct subgroups of astrocyte progenitors at early gliogenesis.

Local proliferation of SPARCL1-marked maturing astrocytes in the ventral forebrain

As the emergence of SPARCL1$^+$ cells in the ventral brain appeared to be earlier than in the dorsal brain, we further examined this lineage in the ventral region of the *Aldh1L1-EGFP* brain sample. Our results showed that SPARCL1 was expressed by almost all EGFP$^+$ astrocyte-lineage cells (Fig. S8A). Co-staining of Ki67 in the E17.5 samples showed that few SPARCL1$^+$ cells at their apparent origin site (the septum-subpallium junction) were positive for Ki67 (Fig. S8B); however, about 40% SPARCL1$^+$ cells in the area beneath the septum-subpallium junction were positive for Ki67 (Fig. S8C). These SPARCL1$^+$Ki67$^+$ cells were likely astrocytes originating from the septum-subpallium junction and migrating to the ventral regions to undergo local proliferation (Fig. S8D), similar to differentiated astrocytes observed in the early postnatal cortex (Ge et al., 2012).

Accumulating evidence indicated that astrocytes in the mouse brain originate from two main sources in multiple waves during early development (Akdemir et al., 2020): one source involves radial glia cells in the late embryonic VZ, which generate astrocytes first through intermediate glial progenitors and then through transforming radial glia (Noctor et al., 2004); another source involves glial progenitors in the perinatal dorsolateral SVZ, which produce astrocytes that subsequently distribute into the cortex and can continue to proliferate at their destination (Ge et al., 2012). Whereas previous studies investigated glial cell heterogeneity in juvenile or adult mouse brain (Marques et al., 2016; John Lin et al., 2017; Lanjakornsiripan et al., 2018; Weng et al., 2019; Batiuk et al., 2020; Bayraktar et al., 2020), our study focused on examination of early heterogeneity of astrocyte lineage cells during embryonic brain development. Our single-cell transcriptome analysis of progenitor cells isolated from the cortex and ganglionic eminence identified two subgroups of APCs, expressing *Sparc* and *Sparcl1*, respectively. Immunohistochemistry results further showed that SPARC$^+$ cells were in the germinal VZ and expressed radial glia progenitor marker *Pax6*. In addition, SPARC staining revealed processes extending from the VZ to cortical pial surface at later stages examined (E18.5 and P1). These results collectively suggested that SPARC$^+$ APCs were most likely radial glia cells that would start the early waves of astrogliogenesis through either producing intermediate astrocyte progenitors or undergoing transformation from neurogenic to gliogenic. The more-prominent presence of *Sparc*-expressing cell cluster (Fig. 1, cluster 5) at the early stage (E15.5) was also consistent with the above idea. On the other hand, SPARCL1$^+$ APCs were initially restricted around the PSB region that would become the future dorsolateral SVZ, as well as around the septum-subpallium junction, indicating that SPARCL1$^+$ APCs were likely the source of the later wave of astrogliogenesis that produced astrocytes that underwent symmetric divisions locally (Ge et al., 2012). In addition, our data showed that the SPARCL1$^+$ progenitor subgroup also had prominent expression of *Egfr* and *Olig2* (Fig. S2), both of which were expressed by OPCs, suggesting that these cells were likely bipotent for becoming astrocytes and oligodendrocytes. Interestingly, a recent study identified a cluster of SPARCL1$^+$EGFR$^+$OLIG2$^+$ cells as the main group of astrocyte progenitors in the developing human cortex, and these cells were found to mainly distribute in the outer SVZ (Fu et al., 2021) – an expanded proliferative region in the

Development (2022) 149, dev199985. doi:10.1242/dev.199985

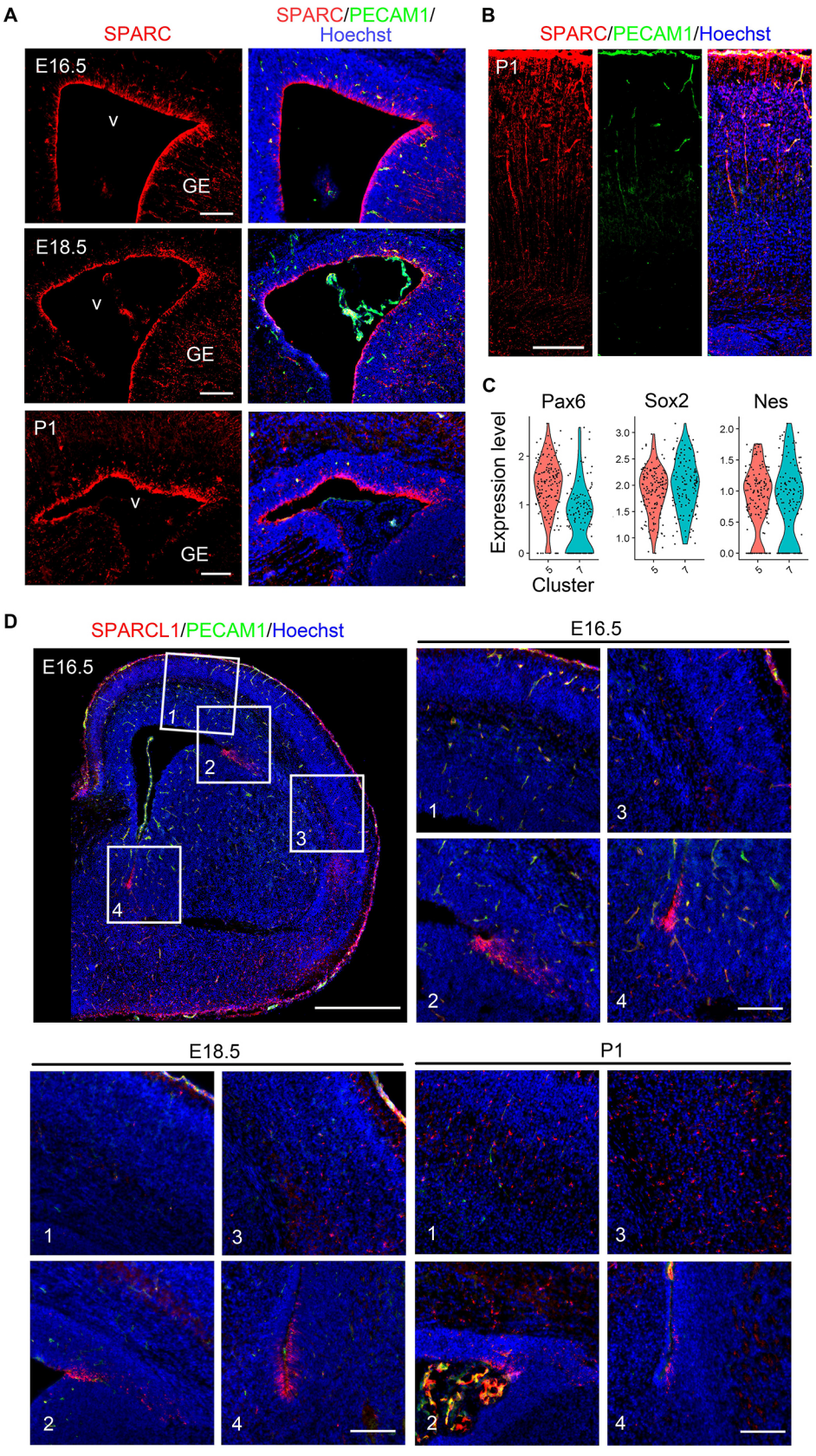

Fig. 2. SPARC and SPARCL1 expression patterns during brain development. (A) Immunostaining of SPARC (red) showed that SPARC was detected prominently lining the ventricular zone. PECAM1/CD31 (green) was used to stain blood vessel cells, which expressed SPARC. Hoechst stains nuclei. v, ventricle; GE, ganglionic eminence. P1, postnatal day 1. Scale bars: 100 µm. (B) Immunostaining of SPARC (red) at P1 showed that SPARC-marked cell processes extended to the cortical pial surface. Scale bar: 100 µm. (C) Violin plots showed *Pax6* had a higher expression in cluster 5 compared with cluster 7 (P=9.48×10^{-14}, Wilcoxon rank sum test), while *Sox2* and *Nes* were expressed at comparable levels in both clusters. (D) SPARCL1 (red) marked ventricular/subventricular zones at the pallium-subpallium boundary (inset 2) in the dorsolateral forebrain and at the septum-subpallium junction (inset 4) in the ventral forebrain. Scale bars: 500 µm in D (top left); 100 µm in D (top right and bottom).

human brain. The fact that the SPARCL1^{+}EGFR^{+}OLIG2^{+} cells have been shown to be the major subgroup of APCs in both the mouse and human brains indicates that there is considerable conservation of astrogliogenesis between the two species.

Our results revealed distinct temporal and spatial patterns of the two subgroups of APCs (Fig. 4G). At the temporal level, two aspects are worth noting. First, SPARC^{+} cells appeared to develop earlier (around E15.5) than SPARCL1^{+} cells (Figs 1E and 3F).

Development (2022) 149, dev199985. doi:10.1242/dev.199985

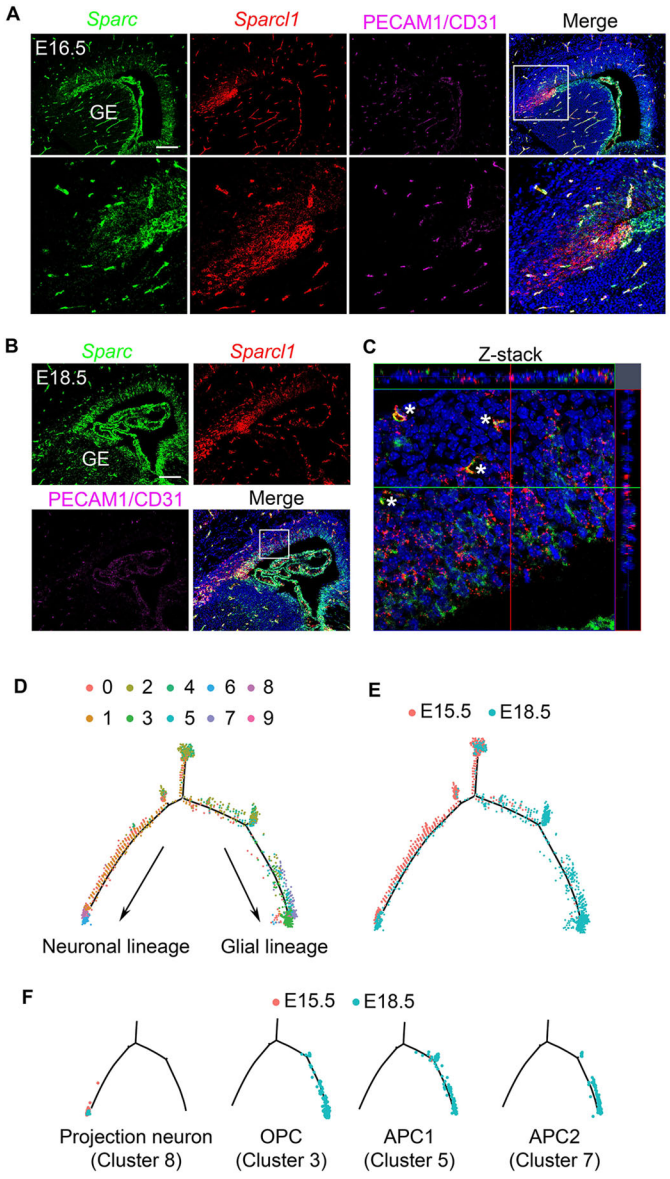

Fig. 3. *Sparc* and *Sparcl1* were expressed in discrete subgroups of APCs. (A,B) *Sparc* (green) and *Sparcl1* (red) were detected at RNA level using RNAscope at E16.5 (A) and E18.5 (B). PECAM1/CD31 antibody (purple) was co-stained to indicate blood vessel cells. GE, ganglionic eminence. Scale bars: 100 µm. (C) High-magnification *z*-stack image of the cortex (outlined in B). Asterisks indicate blood vessel cells. (D-F) Developmental trajectory analyses showed the two astrocyte progenitor subgroups were generated temporally in the cortex. Neural progenitor cells differentiated mainly into neuronal lineage at E15.5 and more prominently into glial lineage at E18.5 (D,E). SPARC-marked APC1 appeared earlier than SPARCL1-marked APC2 (F).

Second, the locations of SPARC$^+$ cells were well demarcated from very early stage (E16.5) through perinatal stages examined; however, the locations of SPARCL1$^+$ cells displayed a dynamic change during development. No SPARCL1$^+$ cells could be detected in the main cortical radial regions at early stages; however, between E18.5 and P1, some SPARCL1$^+$ APCs began to appear in the lateral corner of the cortical VZ, and increasingly more SPARCL1$^+$ cells (presumably differentiated progeny astrocytes) became visible in the cortex spanning from the VZ to the pial surface at P1 (Fig. 2D). It is conceivable that SPARCL1-expressing APCs in the PSB area expanded tangentially and medially into the cortical VZ, and produced astrocytes that subsequently populated the cortex; or, alternatively, some of the cortical VZ radial glia cells became SPARCL1-expressing APCs and produced SPARCL1$^+$ astrocytes that were then dispersed into the cortex. At the spatial level, the two subgroups of APCs were present in separate domains in the ventral brain, with SPARC$^+$ cells residing in the ganglionic eminence region, while SPARCL1$^+$ cells were absent in this region but present in the neighboring areas, centering on the places of origin for these cells (the PSB or septum-subpallium junction). On the other hand, in the dorsal brain region, SPARC$^+$ cells were initially the main APCs detected at an earlier stage (e.g. E16.5). As development progressed, SPARCL1$^+$ APCs emerged in the cortical VZ in an apparent lateral-to-medial gradient from the PSB (Fig. 2D, Fig. S9). Concomitantly, SPARCL1$^+$ astrocytes accumulated and became intermixed with SPARC$^+$ astrocytes in the cortex. Notably, the temporal and spatial patterns of SPARC$^+$ and SPARCL1$^+$ APCs, and their respective progeny astrocytes identified in this study (Fig. 4G), were overall reminiscent of the regional astrocyte allocation revealed by previous fate-mapping studies (Tsai et al., 2012). The biological implication of the distribution difference in the ventral versus dorsal brain between SPARC$^+$ and SPARCL1$^+$ APCs is not clear but might be related to regional functions of these APCs and their progeny astrocytes. In addition, although our data are consistent with SPARC$^+$ and SPARCL1$^+$ cells being APCs, it is possible that these cells may produce other types of glial cell, such as ependymal cells. Future cell fate mapping using *Sparc*- and *Sparcl1*-specific Cre lines will be necessary to define the lineage specifications.

In mature astrocytes, SPARC and SPARCL1 have been found to act as a negative and a positive regulator of synapse formation, respectively (Kucukdereli et al., 2011). This indicates that astrocytes might control the development and plasticity of synapses through regulation of relative levels of SPARC and SPARCL1. Accordingly, it was intriguing that SPARC- and SPARCL1-marked APCs were generated in a temporal sequence during development. The early emergence (by E16.5) of SPARC$^+$ APCs in the VZ (Figs 2A and 4B-D) preceded the establishment of cortical neuronal layers, whereas the later rise and spread of SPARCL1$^+$ APCs from the PSB (Figs 2D and 4E,F; Fig. S9) coincided with the completion of outward migration by most cortical neurons. We speculate that early-generated SPARC$^+$ astrocytes in the cortex might be needed to help prevent premature synapse formation when cortical neurons are still being generated or are in the process of outward migration. In contrast, late-generated SPARCL1$^+$ astrocytes might then be needed to facilitate synapse formation when most neurons are arriving at their destination and the emerging cortical layer structure is being laid out. Further studies are required to examine whether loss of either of the two APC subgroups would compromise the formation of neuronal synapses and the wiring of neural circuits during development.

MATERIALS AND METHODS

Mice

Generation of transgenic mouse lines *Nes-GFP* and *Dcx-mRFP* (The Jackson Laboratory, 024905) have been reported previously (Wang et al., 2011). The transgenic reporter line Aldh1L1-EGFP/Rpl10a was from The Jackson Laboratory (030247) and was maintained as homozygotes without any visible defects. For immunohistochemistry staining experiments, Swiss Webster mice were used if not mentioned specifically. All animals were group housed and maintained in the temperature range and environmental conditions recommended by the American Association for Accreditation of Laboratory Animal Care (AAALAC). Animal procedures were approved by the Institutional Animal Care and Use Committee (IACUC) of the City of

Development (2022) 149, dev199985. doi:10.1242/dev.199985

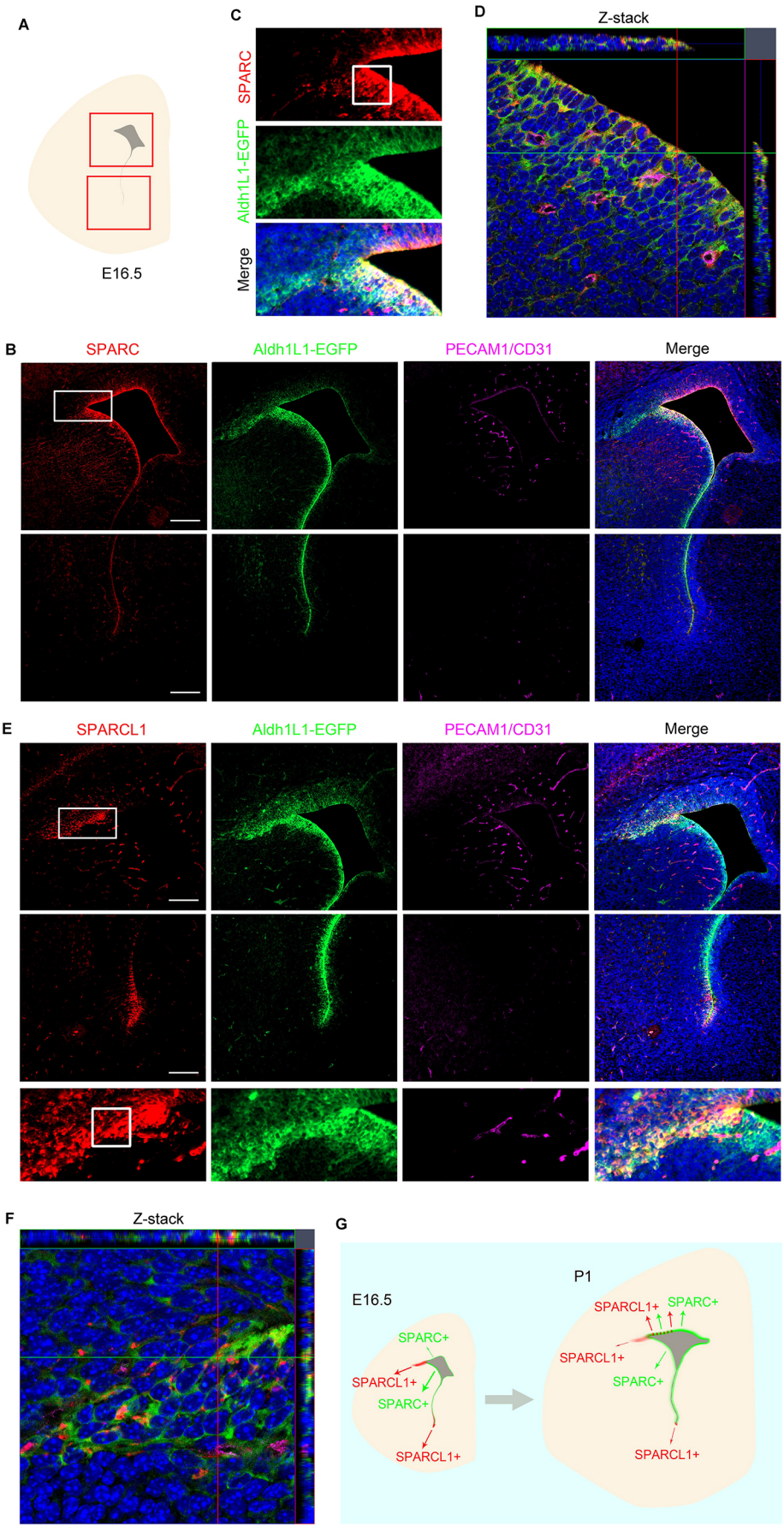

Fig. 4. Distinct APC subgroups marked by SPARC and SPARCL1 at early gliogenesis. (A) Cartoon showing E16.5 brain regions (red boxes) analyzed in B and E. (B) SPARC (red) and EGFP in brains of the *Aldh1L1-EGFP* reporter mice showed overlapping expression lining the VZ. Scale bars: 100 µm. (C) Dorsolateral region (region selected as white box in B) showed EGFP signals, but no SPARC staining in the dorsolateral SVZ area. (D) High-magnification *z*-stack image (region indicated by a white box in C) showed co-expression of EGFP and SPARC. PECAM1/CD31 staining (purple) was applied to indicate blood vessel cells. (E) SPARCL1 (red) and EGFP showed overlapping expression in the dorsolateral SVZ area and at the septum-subpallium junction. Scale bars: 100 µm. (F) High magnification *z*-stack image (region indicated by the white box in E, bottom panel) showed co-expression of EGFP and SPARCL1. PECAM1/CD31 staining (purple) was applied to indicate blood vessel cells. (G) The cartoon illustrates a working model of the temporal and spatial patterns of two APC subgroups in the developing brain. As early as E16.5, SPARC$^+$ APCs are present lining the VZ (green). More SPARC$^+$ cells are detected in the ganglionic eminence region at earlier stages but later on (i.e. P1), SPARC$^+$ cells also accumulate in the cortical region. SPARCL1$^+$ APCs are found in two discrete regions correlating with the pallium-subpallium boundary (PSB) and the septum-subpallium junction, producing SPARCL1$^+$ astrocytes that distribute to the regions nearby. At a later stage (P1), increasing numbers of SPARCL1$^+$ APCs appear in the lateral part of the cortical VZ (indicated in red in the VZ) and concomitantly more SPARCL1$^+$ astrocytes can be seen in the cortex (indicated with red arrows). Distributions of SPARC$^+$ and SPARCL1$^+$ astrocytes in the dorsal and ventral brain regions are strikingly different. The two populations of astrocytes are intermixed in the cortex (indicated by interspersed green and red arrows) but are separated in the ventral brain, where few SPARCL1$^+$ astrocytes can be detected in the ganglionic eminence region.

Development (2022) 149, dev199985. doi:10.1242/dev.199985

Hope and were carried out in accordance with NIH guideline and the Guide for the Care and Use of Laboratory Animals.

Purification of NPCs

For purification of total NPCs, heterozygous *Nes-GFP* mice were bred with homozygous *Dcx-mRFP* mice to yield GFP/RFP double-positive embryos. Pregnant mice were sacrificed at corresponding gestation days (E15.5 and E18.5). The dorsal cortices or ventral forebrain GE regions derived from the double-positive embryos were dissociated by trituration in HBSS (Mediatech) as previously described (Liu et al., 2017). In brief, tissues were dissociated in 15 ml tubes containing 10 ml ice-cold HBSS (with Ca^{2+} and Mg^{2+}) with 5 mM EDTA and 25 µg/ml DNaseI. Tissues were triturated 10 times on ice first, incubated for 5 min and triturated another five times to totally dissociate cells. Cells were centrifuged at 500 ***g*** for 10 min, then resuspended in 10 ml ice-cold HBSS (with Ca^{2+} and Mg^{2+}) containing 12.5 µg/ml DNaseI. After being centrifuged again, cells were finally resuspended in DMEM/F12 medium (Corning, 15-090-CV) containing 12.5 µg/ml DNaseI and 0.5% BSA for sorting. FACS was performed with a four-laser BD FACSAria III System (BD Biosciences). Negative cells, cell debris or cell doublets were excluded with gating of side scatter, forward scatter and pulse width. BD FCASDiva software was used for acquisition and data analysis. Cells were collected into a 1.5 ml microcentrifuge tube containing 500 µl DMEM/F12 with 0.5% BSA.

10X Genomics single-cell RNA-seq

FACS-purified cells were resuspended in PBS containing 0.04% BSA at a concentration of ∼700-1200 cells/µl. Cell number and viability were measured using a TC20 Automated Cell Counter (BioRad). Single-cell RNA libraries were prepared according to the Chromium Single Cell 3′ Reagent Kits v2 User Guide (10X Genomics). Approximately 5000-10,000 cells were loaded on a Chromium Single Cell Controller Instrument (10X Genomics) to generate single-cell gel beads in emulsion (GEMs). The barcoded sequencing libraries were constructed using the Chromium Single-Cell 3′ Library Kit (10X Genomics) for enzymatic fragmentation, end-repair, A-tailing, adaptor ligation, ligation cleanup, sample index PCR and PCR cleanup. Libraries were sequenced with a Hiseq 2500 instrument (Illumina) with a depth of 50,000-100,000 reads per cell.

Analysis of 10X Genomics single-cell RNA-seq data

Raw sequencing data were processed using the 10X Genomics Cell Ranger pipeline (version 1.3.1) to generate FASTQ files and aligned to a mm10 genome to gene expression count. The subsequent data analysis was performed using 'Seurat' package v2.3.0 and R scripts. Cells with mitochondrial read rate >10% and <200 detectable genes were considered as low quality and filtered out. The filtered data were normalized to the total reads of 10,000 for each cell, and regressed to remove the effect of UMI and the percentage of mitochondria genes. The residuals were then mean centered to generate the final scaled data. Normalized and scaled data were clustered using the top principal components of highly variable genes with a resolution of 0.6. The t-distributed stochastic neighbor embedding (t-SNE) algorithm was used to visualize the resulting clusters. Cluster-specific markers were identified to generate heatmap and violin plots in the identified cell clusters using 'Seurat'.

Cross-regional clustering analysis

To identify the similarity of individual clusters across cortex and GE samples, the data from the cortex and GE samples were normalized and standardized using Seurat v2.3.0 as described above. For each identified cell cluster, the average expression of each gene for all the cells in the cluster was calculated using the scaled data. Hierarchical clustering was applied to the average expression data using one correlation as a distance matrix and average linkage algorithm.

Differential expression analyses

To identify differentially expressed (DE) genes across different single-cell clusters, raw data were normalized using 'scran' and compared using Bioconductor package 'MAST'. DE genes were identified using the criteria of a fold change of more than 1.3 and FDR of less than 0.05. Differential expression analysis between cluster 5 and cluster 7 was conducted using 'findMarkers' function implemented in Seurat v4, with a Wilcoxon Rank Sum test. *P* values were adjusted based on Bonferroni correction.

Developmental trajectory

A single-cell trajectory was constructed by Monocle2 (v2.14.0) using the variable features identified by Seurat. A heatmap of the cluster-specific genes along the pseudotime was also generated using Monocle2.

Immunohistochemistry and image processing

The immunohistochemistry staining was caried out as described previously (Hahn et al., 2013). In brief, slides with brain sections (14 µm) were washed three times in PBS, and then incubated in room temperature for 1 h in blocking buffer containing 0.1% Triton X-100, 5% donkey serum (Jackson ImmunoResearch, 017-000-121) and 5% AffiniPure Fab Fragment Donkey anti-mouse IgG (Jackson ImmunoResearch, 715-007-003) in PBS. Sections were then incubated in primary antibody solution containing specific antibodies in PBS with 0.01% Triton X-100 and 1% donkey serum overnight at 4°C. Sections were washed three times in PBS, and donkey-sourced secondary antibodies were diluted in PBS and applied on sections for 2 h in room temperature. Sections were then counterstained by Hoechst 33342 and washed three or four times in PBS. Slides were mounted using Fluoromount-G (SouthernBiotech, 0100-01). Primary antibodies included goat anti-SPARC (R&D Systems, AF942; 1:200), goat anti-SPARCL1 (R&D Systems, AF2836; 1:1000), rat anti-PECAM1/CD31 (BD Biosciences, 550274; 1:200), goat anti-Clu (R&D Systems, AF2747; 1:200), rabbit anti-Ki67 (Abcam, ab16667; 1:200) and rabbit anti-SOX9 (Abcam, ab185966; 1:500). Secondary antibodies with minimal cross-reactivity to other species were purchased from Jackson ImmunoResearch Laboratories: Cy3-donkey anti-goat (705-165-147; 1:400), 488-donkey anti-rat (712-545-150; 1:400), 647-donkey anti-rat (712-605-150; 1:400). Each antibody staining was performed on multiple brain sections and showed consistent patterns. Images were taken using a fluorescence microscope (Zeiss Observer II) or a Zeiss LSM 880 confocal microscope. ZEN software was used for image taking, tiling and processing. Quantification results were presented from three or four brains with five or six sections counted for each brain. Graphs were generated using GraphPad Prism 8.3.0.

RNAscope assay

Sparcl1 and *Sparc* RNA probes were synthesized (Advanced Cell Diagnostics) in fluorescent channels C1 and C2, respectively. RNAscope experiments were performed according to the manuals of RNAscope Multiplex Fluorescent Reagent Kit v2 Assay (Advanced Cell Diagnostics, 323100) and RNA-Protein Co-Detection Ancillary Kit (Advanced Cell Diagnostics, 323180).

Acknowledgements

We thank Jeremy LaDou and Johnathan Garcia for assistance with animal breeding and care; Lucy Brown and Ni Feng for helping with cell sorting; Jinhui Wang and Chao Guo for performing single-cell sequencing; and Brian Armstrong for the use of imaging facility. Research reported in this study included work performed in the Analytical Cytometry Core and the Integrated Genomics Core supported by the National Cancer Institute under award number P30CA033572.

Competing interests

The authors declare no competing or financial interests.

Author contributions

Conceptualization: Q.L., J.L.; Investigation: J.L.; Data curation: J.L., X.W.; Writing - original draft: J.L.; Writing - review & editing: Q.L.; Supervision: Q.L.; Project administration: Q.L.; Funding acquisition: Q.L.

Funding

This work was supported by the National Institutes of Health (NS096130 to Q.L.). Deposited in PMC for release after 12 months.

Data availability

10X Genomics sequencing data have been deposited in GEO under accession number GSE128948.

Peer review history
The peer review history is available online at https://journals.biologists.com/dev/article-lookup/doi/10.1242/dev.199985.

References

Akdemir, E. S., Huang, A. Y. and Deneen, B. (2020). Astrocytogenesis: where, when, and how. *F1000Res* **9**, F1000 Faculty Rev-233. doi:10.12688/f1000research.22405.1

Anderson, S. A., Eisenstat, D. D., Shi, L. and Rubenstein, J. L. (1997). Interneuron migration from basal forebrain to neocortex: dependence on Dlx genes. *Science* **278**, 474-476. doi:10.1126/science.278.5337.474

Batiuk, M. Y., Martirosyan, A., Wahis, J., De Vin, F., Marneffe, C., Kusserow, C., Koeppen, J., Viana, J. F., Oliveira, J. F., Voet, T. et al. (2020). Identification of region-specific astrocyte subtypes at single cell resolution. *Nat. Commun.* **11**, 1220. doi:10.1038/s41467-019-14198-8

Bayraktar, O. A., Fuentealba, L. C., Alvarez-Buylla, A. and Rowitch, D. H. (2014). Astrocyte development and heterogeneity. *Cold Spring Harb. Perspect Biol.* **7**, a020362.

Bayraktar, O. A., Bartels, T., Holmqvist, S., Kleshchevnikov, V., Martirosyan, A., Polioudakis, D., Ben Haim, L., Young, A. M. H., Batiuk, M. Y., Prakash, K. et al. (2020). Astrocyte layers in the mammalian cerebral cortex revealed by a single-cell in situ transcriptomic map. *Nat. Neurosci.* 23, 500-509. doi:10.1038/s41593-020-0602-1

Ben Haim, L. and Rowitch, D. H. (2017). Functional diversity of astrocytes in neural circuit regulation. *Nat. Rev. Neurosci.* **18**, 31-41. doi:10.1038/nrn.2016.159

Clarke, L. E. and Barres, B. A. (2013). Emerging roles of astrocytes in neural circuit development. *Nat. Rev. Neurosci.* **14**, 311-321. doi:10.1038/nrn3484

Fu, Y., Yang, M., Yu, H., Wang, Y., Wu, X., Yong, J., Mao, Y., Cui, Y., Fan, X., Wen, L. et al. (2021). Heterogeneity of glial progenitor cells during the neurogenesis-to-gliogenesis switch in the developing human cerebral cortex. *Cell Rep* **34**, 108788. doi:10.1016/j.celrep.2021.108788

Fuentealba, L. C., Rompani, S. B., Parraguez, J. I., Obernier, K., Romero, R., Cepko, C. L. and Alvarez-Buylla, A. (2015). Embryonic Origin of Postnatal Neural Stem Cells. *Cell* **161**, 1644-1655. doi:10.1016/j.cell.2015.05.041

Ge, W. P., Miyawaki, A., Gage, F. H., Jan, Y. N. and Jan, L. Y. (2012). Local generation of glia is a major astrocyte source in postnatal cortex. *Nature* **484**, 376-380. doi:10.1038/nature10959

Gotz, M. and Huttner, W. B. (2005). The cell biology of neurogenesis. *Nat. Rev. Mol. Cell Biol.* **6**, 777-788. doi:10.1038/nrm1739

Greig, L. C., Woodworth, M. B., Galazo, M. J., Padmanabhan, H. and Macklis, J. D. (2013). Molecular logic of neocortical projection neuron specification, development and diversity. *Nat. Rev. Neurosci.* **14**, 755-769. doi:10.1038/nrn3586

Hahn, M. A., Qiu, R., Wu, X., Li, A. X., Zhang, H., Wang, J., Jui, J., Jin, S. G., Jiang, Y., Pfeifer, G. P. et al. (2013). Dynamics of 5-hydroxymethylcytosine and chromatin marks in Mammalian neurogenesis. *Cell Rep* **3**, 291-300. doi:10.1016/j.celrep.2013.01.011

Hochstim, C., Deneen, B., Lukaszewicz, A., Zhou, Q. and Anderson, D. J. (2008). Identification of positionally distinct astrocyte subtypes whose identities are specified by a homeodomain code. *Cell* **133**, 510-522. doi:10.1016/j.cell.2008.02.046

John Lin, C. C., Yu, K., Hatcher, A., Huang, T. W., Lee, H. K., Carlson, J., Weston, M. C., Chen, F., Zhang, Y., Zhu, W. et al. (2017). Identification of diverse astrocyte populations and their malignant analogs. *Nat. Neurosci.* **20**, 396-405. doi:10.1038/nn.4493

Johnson, M. B., Wang, P. P., Atabay, K. D., Murphy, E. A., Doan, R. N., Hecht, J. L. and Walsh, C. A. (2015). Single-cell analysis reveals transcriptional heterogeneity of neural progenitors in human cortex. *Nat. Neurosci.* **18**, 637-646. doi:10.1038/nn.3980

Khakh, B. S. and Deneen, B. (2019). The emerging nature of astrocyte diversity. *Annu. Rev. Neurosci.* **42**, 187-207. doi:10.1146/annurev-neuro-070918-050443

Kriegstein, A. and Alvarez-Buylla, A. (2009). The glial nature of embryonic and adult neural stem cells. *Annu. Rev. Neurosci.* **32**, 149-184. doi:10.1146/annurev.neuro.051508.135600

Kucukdereli, H., Allen, N. J., Lee, A. T., Feng, A., Ozlu, M. I., Conatser, L. M., Chakraborty, C., Workman, G., Weaver, M., Sage, E. H. et al. (2011). Control of excitatory CNS synaptogenesis by astrocyte-secreted proteins Hevin and SPARC. *Proc. Natl. Acad. Sci. USA* **108**, E440-E449. doi:10.1073/pnas.1104977108

Lanjakornsiripan, D., Pior, B. J., Kawaguchi, D., Furutachi, S., Tahara, T., Katsuyama, Y., Suzuki, Y., Fukazawa, Y. and Gotoh, Y. (2018). Layer-specific morphological and molecular differences in neocortical astrocytes and their dependence on neuronal layers. *Nat. Commun.* **9**, 1623. doi:10.1038/s41467-018-03940-3

Leone, D. P., Srinivasan, K., Chen, B., Alcamo, E. and Mcconnell, S. K. (2008). The determination of projection neuron identity in the developing cerebral cortex. *Curr. Opin. Neurobiol.* **18**, 28-35. doi:10.1016/j.conb.2008.05.006

Li, Z., Tyler, W. A., Zeldich, E., Santpere Baro, G., Okamoto, M., Gao, T., Li, M., Sestan, N. and Haydar, T. F. (2020). Transcriptional priming as a conserved mechanism of lineage diversification in the developing mouse and human neocortex. *Sci. Adv.* **6**, eabd2068. doi:10.1126/sciadv.abd2068

Liu, J., Wu, X., Zhang, H., Qiu, R., Yoshikawa, K. and Lu, Q. (2016). Prospective separation and transcriptome analyses of cortical projection neurons and interneurons based on lineage tracing by Tbr2 (Eomes)-GFP/Dcx-mRFP reporters. *Dev. Neurobiol.* **76**, 587-599. doi:10.1002/dneu.22332

Liu, J., Wu, X., Zhang, H., Pfeifer, G. P. and Lu, Q. (2017). Dynamics of RNA polymerase II pausing and bivalent histone H3 methylation during neuronal differentiation in brain development. *Cell Rep* **20**, 1307-1318. doi:10.1016/j.celrep.2017.07.046

Liu, J., Geng, A., Wu, X., Lin, R. J. and Lu, Q. (2018). Alternative RNA splicing associated with mammalian neuronal differentiation. *Cereb. Cortex* **28**, 2810-2816. doi:10.1093/cercor/bhx160

Loo, L., Simon, J. M., Xing, L., Mccoy, E. S., Niehaus, J. K., Guo, J., Anton, E. S. and Zylka, M. J. (2019). Single-cell transcriptomic analysis of mouse neocortical development. *Nat. Commun.* **10**, 134. doi:10.1038/s41467-018-08079-9

Marques, S., Zeisel, A., Codeluppi, S., Van Bruggen, D., Mendanha Falcao, A., Xiao, L., Li, H., Haring, M., Hochgerner, H., Romanov, R. A. et al. (2016). Oligodendrocyte heterogeneity in the mouse juvenile and adult central nervous system. *Science* **352**, 1326-1329. doi:10.1126/science.aaf6463

Mi, D., Li, Z., Lim, L., Li, M., Moissidis, M., Yang, Y., Gao, T., Hu, T. X., Pratt, T., Price, D. J. et al. (2018). Early emergence of cortical interneuron diversity in the mouse embryo. *Science* **360**, 81-85. doi:10.1126/science.aar6821

Molofsky, A. V. and Deneen, B. (2015). Astrocyte development: a guide for the perplexed. *Glia* **63**, 1320-1329. doi:10.1002/glia.22836

Noctor, S. C., Martinez-Cerdeno, V., Ivic, L. and Kriegstein, A. R. (2004). Cortical neurons arise in symmetric and asymmetric division zones and migrate through specific phases. *Nat. Neurosci.* **7**, 136-144. doi:10.1038/nn1172

Okamoto, M., Miyata, T., Konno, D., Ueda, H. R., Kasukawa, T., Hashimoto, M., Matsuzaki, F. and Kawaguchi, A. (2016). Cell-cycle-independent transitions in temporal identity of mammalian neural progenitor cells. *Nat. Commun.* **7**, 11349. doi:10.1038/ncomms11349

Polioudakis, D., De, L. A., Torre-Ubieta, L., Langerman, J., Elkins, A. G., Shi, X., Stein, J. L., Vuong, C. K., Nichterwitz, S., Gevorgian, M. et al. (2019). A single-cell transcriptomic atlas of human neocortical development during mid-gestation. *Neuron* **103**, 785-801. doi:10.1016/j.neuron.2019.06.011

Pollen, A. A., Nowakowski, T. J., Chen, J., Retallack, H., Sandoval-Espinosa, C., Nicholas, C. R., Shuga, J., Liu, S. J., Oldham, M. C., Diaz, A. et al. (2015). Molecular identity of human outer radial glia during cortical development. *Cell* **163**, 55-67. doi:10.1016/j.cell.2015.09.004

Rowitch, D. H. and Kriegstein, A. R. (2010). Developmental genetics of vertebrate glial-cell specification. *Nature* **468**, 214-222. doi:10.1038/nature09611

Shin, J., Berg, D. A., Zhu, Y., Shin, J. Y., Song, J., Bonaguidi, M. A., Enikolopov, G., Nauen, D. W., Christian, K. M., Ming, G. L. et al. (2015). Single-cell RNA-seq with waterfall reveals molecular cascades underlying adult neurogenesis. *Cell Stem Cell* **17**, 360-372. doi:10.1016/j.stem.2015.07.013

Sloan, S. A. and Barres, B. A. (2014). Mechanisms of astrocyte development and their contributions to neurodevelopmental disorders. *Curr. Opin. Neurobiol.* **27**, 75-81. doi:10.1016/j.conb.2014.03.005

Suzuki, S., Namiki, J., Shibata, S., Mastuzaki, Y. and Okano, H. (2010). The neural stem/progenitor cell marker nestin is expressed in proliferative endothelial cells, but not in mature vasculature. *J. Histochem. Cytochem.* **58**, 721-730. doi:10.1369/jhc.2010.955609

Tabata, H. (2015). Diverse subtypes of astrocytes and their development during corticogenesis. *Front. Neurosci.* **9**, 114. doi:10.3389/fnins.2015.00114

Telley, L., Agirman, G., Prados, J., Amberg, N., Fievre, S., Oberst, P., Bartolini, G., Vitali, I., Cadilhac, C., Hippenmeyer, S. et al. (2019). Temporal patterning of apical progenitors and their daughter neurons in the developing neocortex. *Science* **364**, eaav2522. doi:10.1126/science.aav2522

Tien, A. C., Tsai, H. H., Molofsky, A. V., Mcmahon, M., Foo, L. C., Kaul, A., Dougherty, J. D., Heintz, N., Gutmann, D. H., Barres, B. A. and et al. (2012). Regulated temporal-spatial astrocyte precursor cell proliferation involves BRAF signalling in mammalian spinal cord. *Development* **139**, 2477-2487. doi:10.1242/dev.077214

Tsai, H. H., Li, H., Fuentealba, L. C., Molofsky, A. V., Taveira-Marques, R., Zhuang, H., Tenney, A., Murnen, A. T., Fancy, S. P., Merkle, F. et al. (2012). Regional astrocyte allocation regulates CNS synaptogenesis and repair. *Science* **337**, 358-362. doi:10.1126/science.1222381

Wang, J., Zhang, H., Young, A. G., Qiu, R., Argalian, S., Li, X., Wu, X., Lemke, G. and Lu, Q. (2011). Transcriptome analysis of neural progenitor cells by a genetic dual reporter strategy. *Stem Cells* **29**, 1589-1600. doi:10.1002/stem.699

Weng, Q., Wang, J., Wang, J., He, D., Cheng, Z., Zhang, F., Verma, R., Xu, L., Dong, X., Liao, Y. et al. (2019). Single-cell transcriptomics uncovers glial progenitor diversity and cell fate determinants during development and gliomagenesis. *Cell Stem Cell* **24**, 707-723.

Wu, S., Esumi, S., Watanabe, K., Chen, J., Nakamura, K. C., Nakamura, K., Kometani, K., Minato, N., Yanagawa, Y., Akashi, K. et al. (2011). Tangential

migration and proliferation of intermediate progenitors of GABAergic neurons in the mouse telencephalon. *Development* **138**, 2499-2509. doi:10.1242/dev.063032

Yuzwa, S. A., Borrett, M. J., Innes, B. T., Voronova, A., Ketela, T., Kaplan, D. R., Bader, G. D. and Miller, F. D. (2017). Developmental emergence of adult neural stem cells as revealed by single-cell transcriptional profiling. *Cell Rep* **21**, 3970-3986. doi:10.1016/j.celrep.2017.12.017

Zeisel, A., Munoz-Manchado, A. B., Codeluppi, S., Lonnerberg, P., La Manno, G., Jureus, A., Marques, S., Munguba, H., He, L., Betsholtz, C. et al. (2015). Brain structure. Cell types in the mouse cortex and hippocampus revealed by single-cell RNA-seq. *Science* **347**, 1138-1142. doi:10.1126/science.aaa1934

Zeisel, A., Hochgerner, H., Lonnerberg, P., Johnsson, A., Memic, F., Van Der Zwan, J., Haring, M., Braun, E., Borm, L. E., La Manno, G. et al. (2018). Molecular architecture of the mouse nervous system. *Cell* **174**, 999-1014. doi:10.1016/j.cell.2018.06.021

Zhong, S., Zhang, S., Fan, X., Wu, Q., Yan, L., Dong, J., Zhang, H., Li, L., Sun, L., Pan, N. et al. (2018). A single-cell RNA-seq survey of the developmental landscape of the human prefrontal cortex. *Nature* **555**, 524-528. doi:10.1038/nature25980

Fig. S1

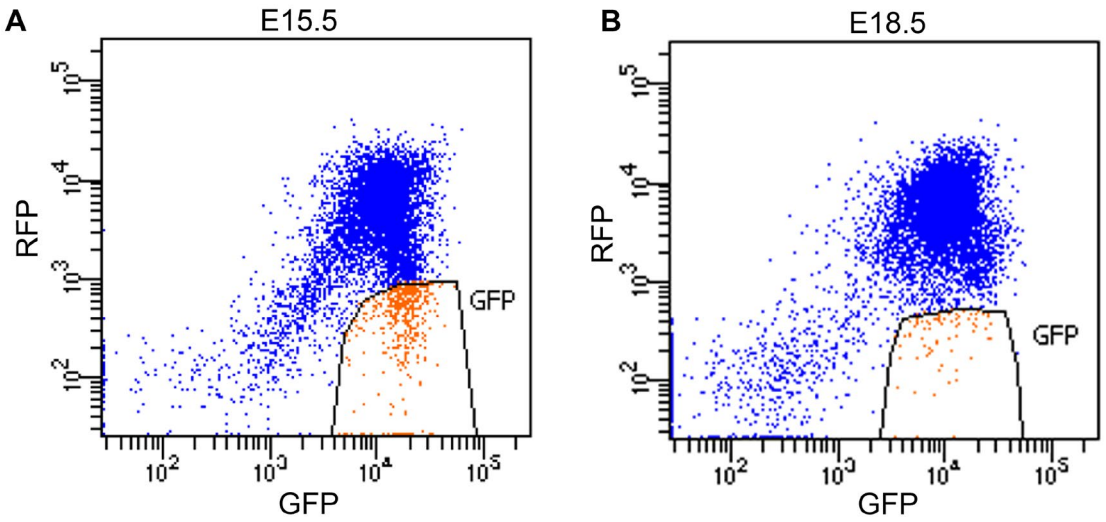

Fig. S1. FACS profiles for purification of neural progenitor cells (NPCs) from cortex at E15.5 (A) and E18.5 (B).
After excluding cell debris and cell doublets, NPCs (GFP^+RFP^-, cell dot regions in orange) were collected for 10X Genomics single-cell RNA sequencing analysis.

Fig. S2

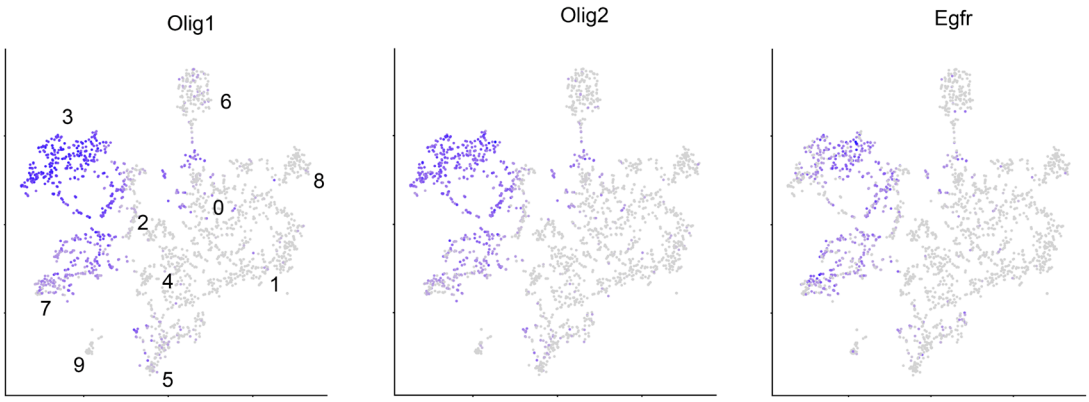

Fig. S2. t-SNE plots of *Olig1, Olig2* and *Egfr* in cortical NPC subgroups.
All 3 markers (*Olig1, Olig2* and *Egfr*) of oligodendrocyte progenitor cells (OPCs) showed relatively higher expression level in cluster 7 astrocyte progenitor cell (APC) subgroup than in cluster 5 APC subgroup. Numbers 0-9 represent the same clusters as in **Figure 1**.

Fig. S3

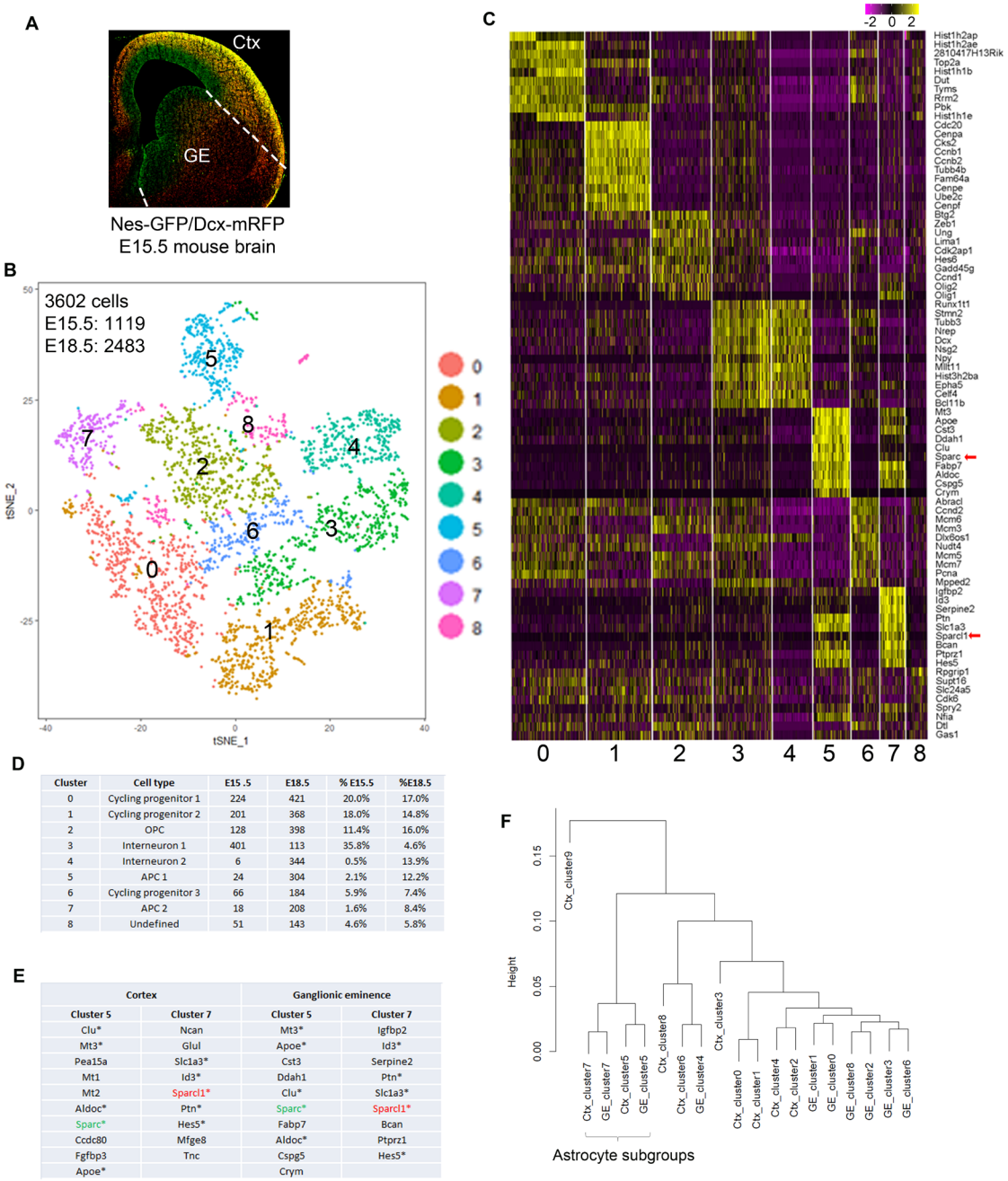

D

Cluster	Cell type	E15 .5	E18.5	% E15.5	%E18.5
0	Cycling progenitor 1	224	421	20.0%	17.0%
1	Cycling progenitor 2	201	368	18.0%	14.8%
2	OPC	128	398	11.4%	16.0%
3	Interneuron 1	401	113	35.8%	4.6%
4	Interneuron 2	6	344	0.5%	13.9%
5	APC 1	24	304	2.1%	12.2%
6	Cycling progenitor 3	66	184	5.9%	7.4%
7	APC 2	18	208	1.6%	8.4%
8	Undefined	51	143	4.6%	5.8%

E

Cortex		Ganglionic eminence	
Cluster 5	Cluster 7	Cluster 5	Cluster 7
Clu*	Ncan	Mt3*	Igfbp2
Mt3*	Glul	Apoe*	Id3*
Pea15a	Slc1a3*	Cst3	Serpine2
Mt1	Id3*	Ddah1	Ptn*
Mt2	Sparcl1*	Clu*	Slc1a3*
Aldoc*	Ptn*	Sparc*	Sparcl1*
Sparc*	Hes5*	Fabp7	Bcan
Ccdc80	Mfge8	Aldoc*	Ptprz1
Fgfbp3	Tnc	Cspg5	Hes5*
Apoe*		Crym	

Fig. S3. Two astrocyte progenitor subgroups identified from the ventral forebrain by scRNA-seq.

A Image shows *Nes-GFP/Dcx-mRFP* brain section at E15.5. The dissected ganglionic eminence (GE) region of the ventral forebrain was indicated (white dash lines). Ctx, cortex.

B t-SNE plot of 3602 single cells at E15.5 and E18.5 after NPC enrichment and quality control filter from 10X Genomics scRNA-seq. Nine clusters (cluster 0 to 8) were identified.

C Heatmap of the single cell clusters. Representative genes of each cluster were shown. *Sparc* and *Sparcl1* were marked (red arrows).

D Summary of cell types, cell numbers and ratios at E15.5 and E18.5. OPC, oligodendrocyte progenitor cell; APC, astrocyte progenitor cell.

E Representative genes of astrocyte progenitor subgroups from the cortex and ganglionic eminence. Same genes between the subgroups were labeled with (*). *Sparc* was labeled in green and *Sparcl1* in red.

F Cross-regional clustering analysis of astrocyte progenitor subgroups expressing *Sparc* or *Sparcl1*.

Fig. S4

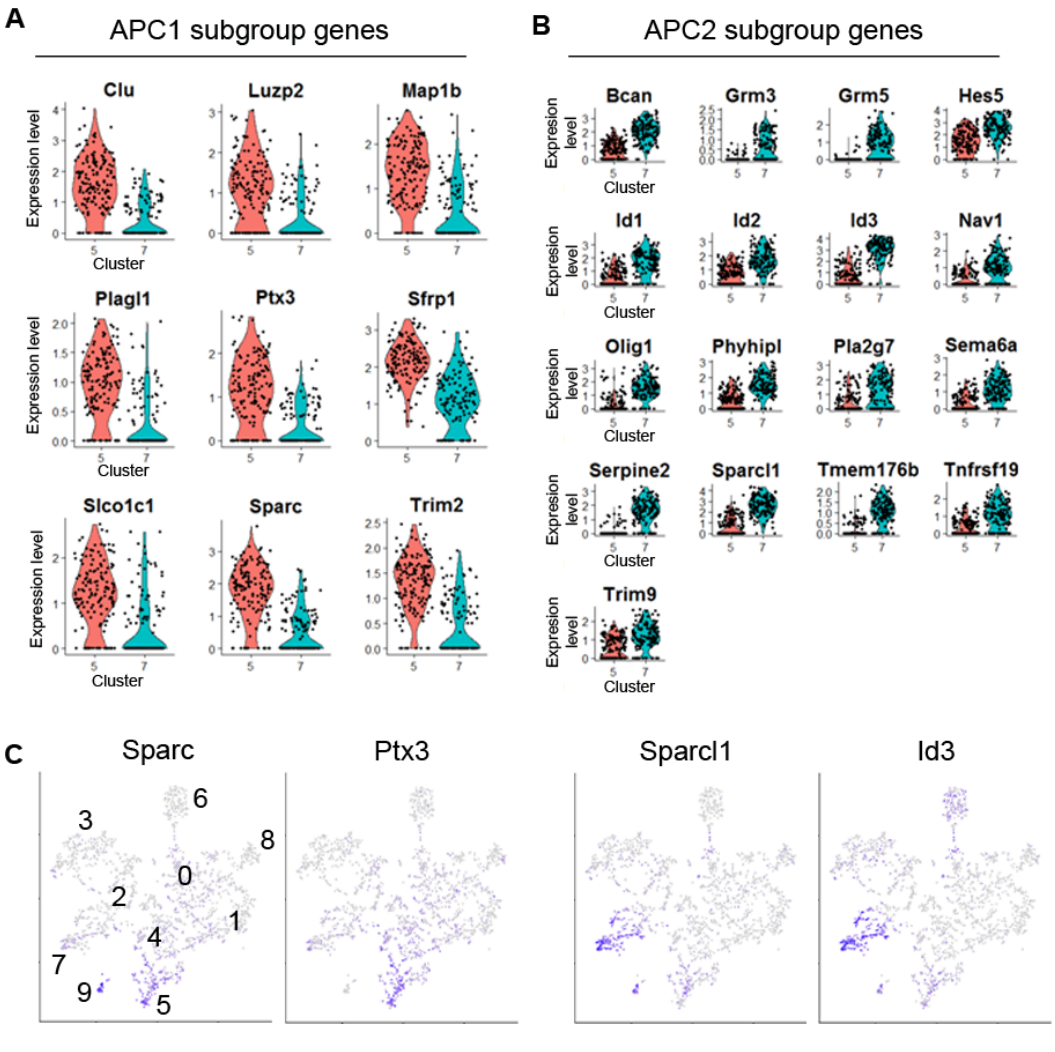

Fig. S4. Differentially expressed genes between two astrocyte progenitor subgroups from the cortex.
A Violin plots of differentially expressed genes in the *Sparc*-expressing progenitors (Cluster 5, APC1).
B Violin plots of differentially expressed genes in the *Sparcl1*-expressing progenitors (Cluster 7, APC2).
C t-SNE plots of representative genes.

Fig. S5

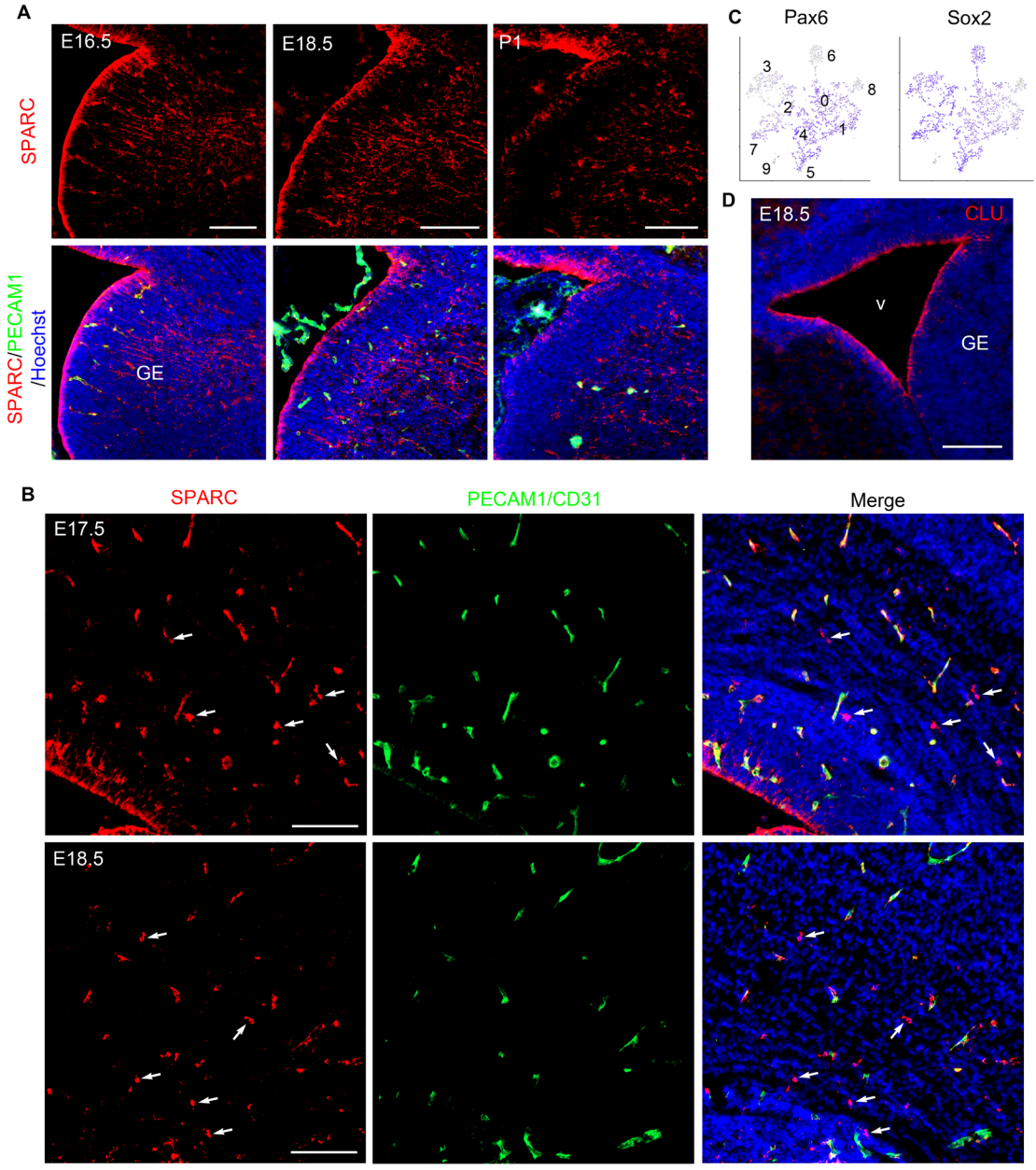

Fig. S5. SPARC$^+$ cells in the cortical regions.
A Immunostaining of SPARC (red) in ganglionic eminence (GE) regions. Scale bars: 100 μm.
B SPARC staining (red) detected cells lining the ventricle (APCs) and cells outside the ventricular zone (indicated by white arrows in the red and merged panels; presumably differentiating astrocytes). PECAM1/CD31 (green) was used to stain blood vessel cells which expressed SPARC. Scale bars: 100 μm.
C t-SNE plots of *Pax6* and *Sox2* showed that *Pax6* level was relatively higher in *Sparc*-expressing cluster 5, whereas *Sox2* was at a similar level in both clusters 5 and 7.
D Antibody staining showed that CLU protein was expressed lining the ventricle (v) at E18.5, similar with SPARC staining. GE, ganglionic eminence. Scale bar: 100 μm.

Fig. S6

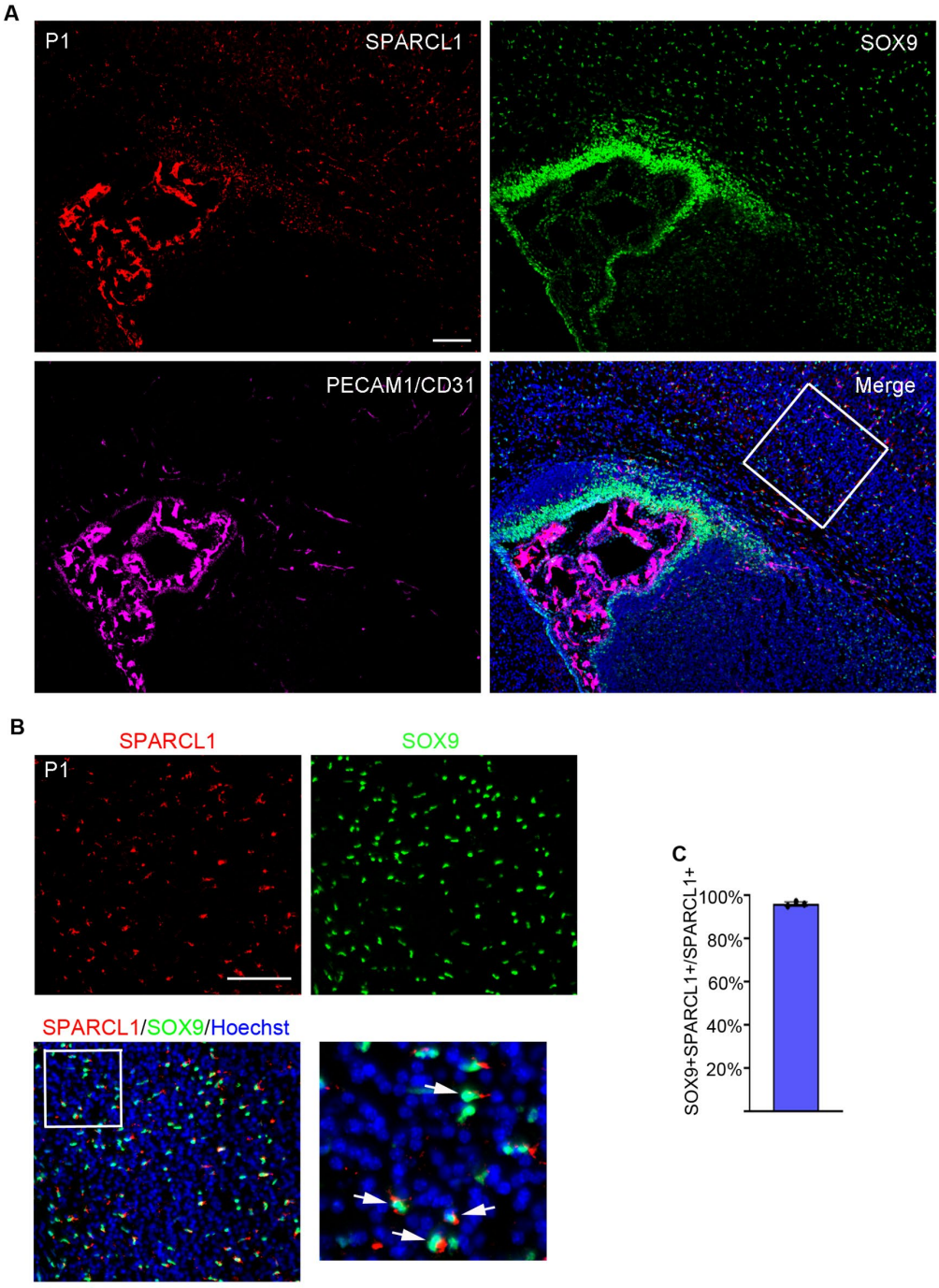

Fig. S6. Co-expression of SPARCL1 with SOX9.
A SPARCL1-expressing cells (red) showed co-expression with glial-lineage progenitor marker SOX9 (green). Scale bar: 100 μm.
B Region selected from the boxed area indicated in panel (A). White arrows indicate secreted SPARCL1(red)-associated SOX9(green) positive cells. Scale bar: 100 μm.
C Quantification of SOX9+ cells from SPARCL1+ cells (An average of 124/129; N=3).

Fig. S7

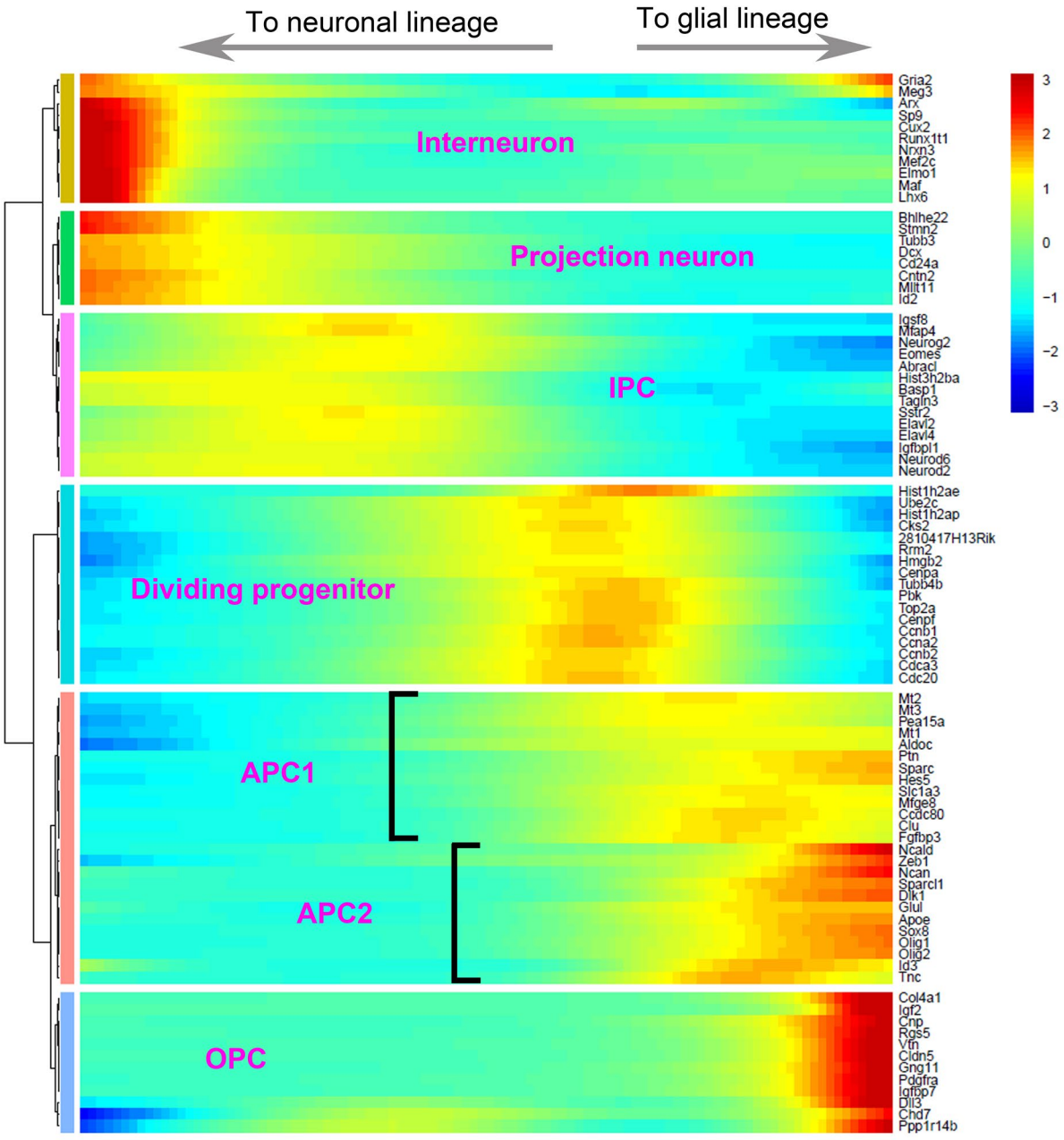

Fig. S7. Heatmap of the cluster specific genes along the pseudotime.
Heatmap of the cluster specific genes along the pseudotime displayed a clear pattern that one side with neuronal lineages related genes and another side with glial lineage related genes, and that *Sparc*-marked APC1 genes were expressed earlier than *Sparcl1*-marked APC2 genes. IPC, intermediate progenitor cell; APC, astrocyte progenitor cell; OPC, oligodendrocyte progenitor cell.

Fig. S8

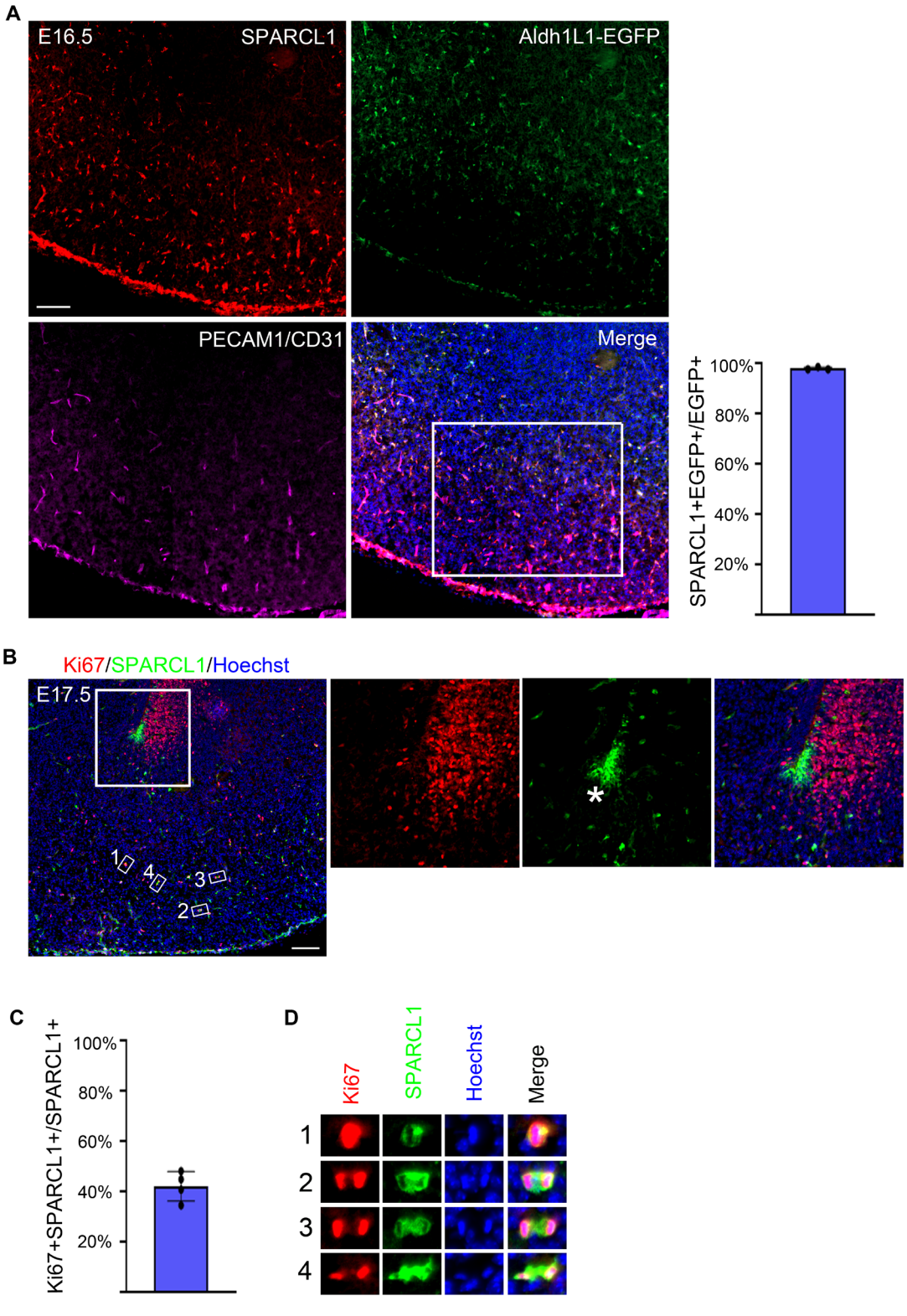

Fig. S8. Local proliferation of SPARCL1-expressing astrocytes in the ventral forebrain.
A Immunostaining of SPARCL1 (red) on the E16.5 brain sections of the *Aldh1L1-EGFP* reporter mice showed that in the region ventral to the septum-subpallium junction, SPARCL1 was detected in almost all EGFP-positive cells, which were likely differentiated astrocytes. Scale bar: 100 μm. White box indicated the region for quantification. Right column, quantification of non-blood vessel (PECAM1/CD31 negative) SPARCL1$^+$ cells in EGFP$^+$ cells (An average of 84/86; N=3).
B At E17.5, Ki67 signals (red) were absent in SPARCL1$^+$ cells originated at the septum-subpallium junction (asterisk), but around 40% non-blood vessel (PECAM1/CD31 negative) SPARCL1$^+$ were Ki67$^+$ beneath septum-subpallium junction. Four such dividing cells were labeled out (boxes 1-4). Scale bar: 100 μm.
C Quantification of Ki67$^+$ cells in non-blood vessel (PECAM1/CD31 negative) SPARCL1$^+$ cells (An average of 37/86; N=4).
D Representative dividing cells from metaphase to late anaphase were shown from panel **B**.

Fig. S9

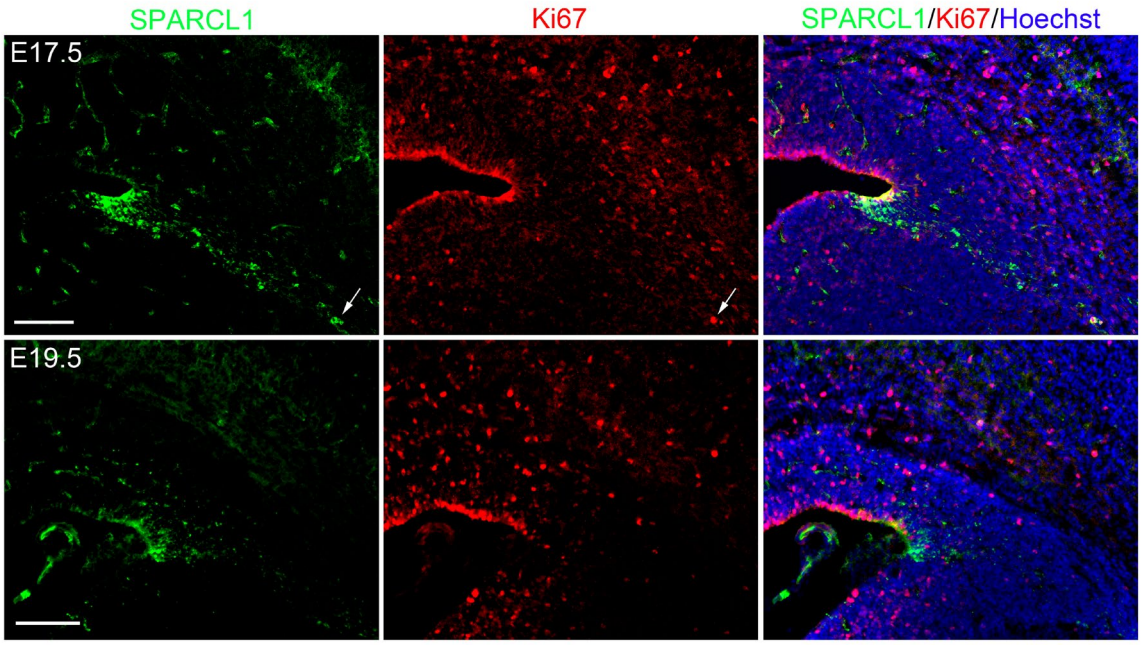

Fig. S9. Temporal patterns of SPARCL1⁺ APCs around PSB and cortical VZ.
At E17.5 (or earlier), SPARCL1⁺ APCs were prominently seen in the ventral side of pallium-subpallium boundary (PSB). Proliferating (Ki67⁺) APCs were enriched at the apical surface. Some SPARCL1⁺ cells appeared to stream out towards lateral-ventral areas; these were likely differentiating astrocytes originated from the PSB and they might later undergo local proliferation (arrow). At around birth (E19.5), SPARCL1⁺ APCs appeared to be mainly seen in the dorsal side of the PSB and distribute medially into the cortex proper. Fewer proliferating APCs were present at the apical surface at this stage. Scale bars: 100 μm.